Universiteit
Leiden
The Netherlands

Clues from stellar catastrophes

Rimoldi, A.J.

Citation
Rimoldi, A. J. (2016, March 29). *Clues from stellar catastrophes*. Retrieved from https://hdl.handle.net/1887/38640

Version:	Not Applicable (or Unknown)
License:	Leiden University Non-exclusive license
Downloaded from:	https://hdl.handle.net/1887/38640

Note: To cite this publication please use the final published version (if applicable).

Cover Page

Universiteit Leiden

The handle http://hdl.handle.net/1887/38640 holds various files of this Leiden University dissertation

Author: Rimoldi, Alexander
Title: Clues from stellar catastrophes
Issue Date: 2016-03-29

5 A method to infer globular cluster evolution from observations of blue stragglers: the case of Hodge 11

A. Rimoldi, S. F. Portegies Zwart, E. M. Rossi
To be submitted

Blue straggler stars (BSSs) are ubiquitous in galactic globular clusters. Sitting above the main sequence turn-off, BSSs appear younger than the rest of the cluster. Two formation channels are often proposed to explain their origin: collisions between stars and binary mass transfer. The former is more likely at higher stellar densities, and therefore in particular after a cluster has undergone core collapse. We study the possible collisional origin of 24 of the innermost BSSs in the 11.7 Gyr–old Large Magellanic Cloud globular cluster Hodge 11, and use the derived collision times to estimate the time of cluster core collapse. To construct model BSSs, we adopt masses for hypothetical pairs of stars and collision times. We then use stellar evolution and collision codes in the Astrophysical Multipurpose Software Environment to evolve the two stars to the moment of collision, merge them, and then evolve the collision product to the age of the cluster. For each observed BSS, we find the best fitting collision time and the masses of the two merging stars. The results show that the distribution of mass between the two colliding stars has some degeneracy, but the time at which they collide is better defined. The formation rate of BSSs can be described well by the superposition of a constant background rate of 1.7 Gyr^{-1} and an exponentially decaying function with a peak at 3.4 Gyr (corresponding to the BSSs nearest to the turn-off) and an e-folding time of 1.4 Gyr. We attribute the background contribution to binary mass transfer and coalescence, which are not particularly sensitive to the dynamical evolution of the star cluster. The exponential rate we attribute to dynamically induced stellar collisions during the core collapse of the globular cluster. The expected moment of core collapse for Hodge 11 is then consistent with the peak of the exponential function (or somewhat earlier). The relatively long decay in the exponential curve may then be attributed to an episode of gravothermal oscillations, persisting for more than a Gyr.

5.1 Introduction

Since their discovery in the globular cluster M3, blue straggler stars (BSSs; Sandage 1953) have been a popular indicator for the dynamical evolution of stellar clusters (Stryker 1993; Bailyn 1995; Ferraro 2015). The two leading mechanisms for their origin involve collisions between stars in the cluster (Hills and Day 1976) and mass transfer (or coalescence) in binary stars (McCrea 1964). Both of these processes rejuvenate the star with respect to its surroundings, because they tend to make the star more massive, and fresh hydrogen may be mixed in the stellar interior, extending its main sequence lifetime. As a consequence, both processes lead to a population of stars that appear to be younger (born at a later epoch) that the other cluster members. It turns out to be difficult to objectively make a distinction between these two origin processes, and both are expected to contribute to the formation of BSSs (Davies 2015). Slight differences in the response to the moment at which mass is added, and subtleties in the stellar evolution, depending on how the stellar mass increases, give rise to slight differences in the observational characteristics (Ferraro et al. 2015).

We will test and study the consequences of the hypothesis that BSSs are the result of a collision between two stars, and use this to make inferences about the dynamical evolution of a globular cluster. As a template BSS population, we adopt those observed with the *Hubble Space Telescope* (HST) in the Large Magellanic Cloud cluster Hodge 11 (Li et al. 2013). The 162 BSSs in this $11.7^{+0.2}_{-0.1}$ Gyr-old star cluster appear to be composed of two distinct populations. The innermost BSSs, in the cluster core region (27 stars, at ≤ 15 arc seconds), are systematically lower in the colour-magnitude space (see Fig. 5.1) than the outermost subsample (also 27 stars, between 85 and 100 arc seconds; Li et al. 2013). This difference in color is consistent with earlier calculations on the origin of BSSs from direct stellar collisions, which tend to produce fainter BSSs that are rather close to the zero-age main sequence compared to those from a binary mass-transfer origin (Portegies Zwart et al. 1997a,b; Sills et al. 2002). This distinction is consistent with the collisional (blue) BSSs being in the densest regions where most collisions tend to occur, whereas outside the core it is suggested that binary evolution processes are dominant (Davies et al. 2004). Although stellar collisions tend to occur in the core, this collision rate increases sharply when the cluster experiences a phase of core collapse.

The ~ 40 BSSs in the globular cluster NGC 1261 show a similar bimodal distribution of red and blue BSSs. The latter population tend to be slightly more concentrated than the former, and both populations are more concentrated than the subgiants in the cluster. The blue BSS population was attributed to a core collapse in the star cluster, which, according to single stellar evolution models should have occurred about 200 Myr ago (Simunovic et al. 2014). Simunovic et al. (2014) adopted single stellar evolution models to study the BSS population in the Hertzsprung-Russell (HR) diagram, and correlate them with the moment of core collapse.

Our approach is similar in terms of using the blue BSSs to find the moment of

core collapse in Hodge 11. As we are interested in a population with the highest likelihood to have been formed from stellar collisions, we focus here on the innermost subsample of 27 BSSs in Hodge 11 (though we will also compare our results with the outermost subsample). However, instead of a more straightforward HR diagram analysis, we take the approach of simulating the collision process of the stars in order to reconstruct the histories of individual BSSs in the cluster. We approach the problem in two ways. We first create a grid of initial conditions to predict the final HST V and $V-I$ magnitudes, on which we fit the sample of BSSs by interpolation. As a second approach, the collision components for some selected BSSs are estimated by means of a Markov-Chain Monte Carlo (MCMC) method, in which the observed V and $V-I$ magnitudes of each BSS, as well as the age of the cluster, are used as goodness-of-fit parameters in the optimization algorithm. We compare the results of the two methods, providing a validation of our MCMC method by means of the gridded data.

5.2 Method

For both the MCMC and grid approaches, we employ the same method of generating a BSS. We first outline this method of creating BSS models and how the stellar properties are converted into observational predictions. We then discuss the two approaches in applying these predictions to the observed data.

5.2.1 BSS models

In order to construct each BSS model, we employ two astrophysics codes within the Astrophysical Multipurpose Software Environment (`AMUSE`; Portegies Zwart et al. 2009, 2013a). We start by constructing internal stellar structure models of two component stars with masses M_1 and M_2 using the Henyey code `MESA` (Paxton et al. 2011). The two stars are initialised with a metallicity of $Z = 0.0002$ ([Fe/H] ≈ -1.98), representative of the low birth metallicity of the globular cluster stars (Li et al. 2013). Both of these stars are then evolved to identical ages, representing the collision time $t_{\rm col}$. Agreement of the ages is achieved by constraining the final time steps applied by `MESA`; if the internally-determined `MESA` time steps are used, they are typically too coarse on the main sequence to get agreement of the final two stellar ages.

Once the stellar structure models have been constructed, we then merge the two stars using a second code in `AMUSE`, Make-Me-A-Massive-Star (`MMAMS`; Gaburov et al. 2008). `MMAMS` uses an entropy-sorting algorithm to determine the new equilibrium of a stellar collision, which extends a method first used for low-mass main sequence star collisions (Lombardi et al. 1996, 2002, 2003). This method of calculating the stellar structure typically takes a few minutes to produce a result, which allows us to perform a large sample of parameter space. A parameter search using full hydrodynamic simulations of such collisions would be infeasible, as the equivalent calculations can take a day or more on the same hardware (Gaburov et al. 2008). Finally, once the collision

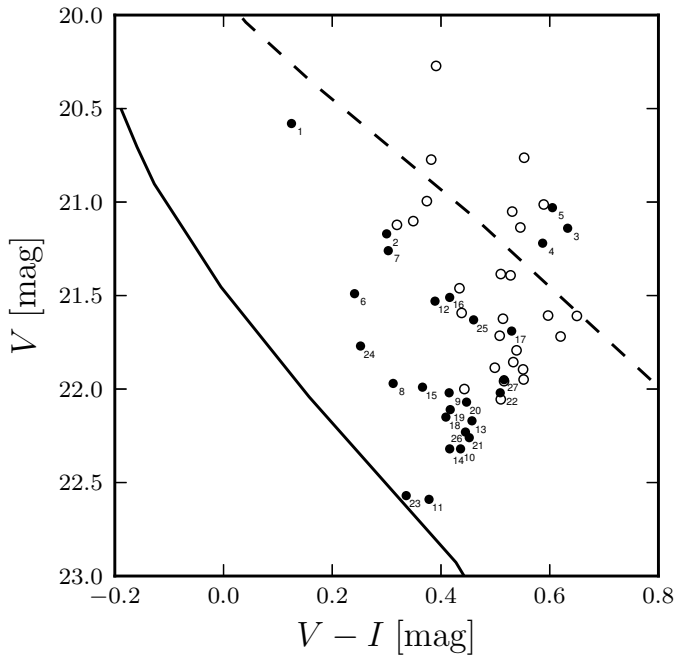

Figure 5.1: Positions on the colour-magnitude diagram for all the BSSs in Hodge 11. Bullets correspond to the inner population ($\leq$ 15 arc seconds) of 27 BSSs (see Table 5.1), and open circles correspond to the outer population (between 85 and 100 arc seconds) of 27 BSSs. The solid black line shows the single-star zero-age main sequence as calculated in `MESA` with metallicity $Z = 0.0002$ and converted to V and $V - I$ space as described in Section 5.2.1. The dashed black line shows the terminal-age main sequence, as reported by `AMUSE` for the `MESA` models. The inner points are numbered corresponding to Table 5.1.

product has been generated, it is loaded back into `MESA`, and this BSS is then evolved until the age of the cluster.

Conversion from simulation results to observational parameters

Once we have produced a BSS model from `MESA` and `MMAMS`, we need to determine the equivalent V and I magnitudes in order to compare with observed BSSs. To do so, we have adapted a code used in Martínez-Barbosa et al. (2016), which was originally developed for predictions of *Gaia* magnitudes from simulated solar siblings in the Milky Way, and interfaced it with our blue-straggler code. We have modified this code to use the HST WFPC2 camera passbands[1] F555W and F814W (the V and I equivalent bands) that were used in the observations of Li et al. (2013).

[1]The response functions were obtained at: `ftp://ftp.stsci.edu/cdbs/comp/wfpc2/`

Given a stellar structure model from MESA, we first find a best-match stellar spectrum from the BaSeL database of stellar spectra (Westera et al. 2002). We then perform a convolution of this spectrum with each filter response function in order to obtain a flux. This flux in each band is then converted to an observed magnitude by applying both a (true) distance modulus ($\mu_0 = 18.5$; Alves 2004; Li et al. 2013), as well as an extinction, where we use a colour excess of $E(B-V) = 0.09$ for Hodge 11 (Li et al. 2013) along with the $A/E(B-V)$ conversions to the two WFPC2 bands in Schlegel et al. (1998). This gives the final 'observed' V and I magnitudes from the simulation, which can then be directly compared with the observational HST data.

In Fig. 5.1, we overlay the single-star zero-age main sequence (ZAMS; solid line) and terminal-age main sequence (TAMS; dashed line) from $Z = 0.0002$ models in MESA, converted to V and $V-I$ using this method, on the colour-magnitude diagram (CMD) of the observed Hodge 11 BSSs. A star is flagged as having left the main sequence (therefore having reached the TAMS) if, according to MESA, the core hydrogen fraction reaches 1 per cent and the core temperature is dropping.

5.2.2 Grid approach

The grid was generated using an $8\times27\times24$ array of initial conditions over the respective intervals of $0.5\ M_\odot \leq M_1 \leq 0.85\ M_\odot$, $0.2\ M_\odot \leq M_2 \leq 0.85\ M_\odot$ and $0.1 \leq t_{\rm col} \leq 11.7$ Gyr. The grid is immediately reduced in size along the M_2 dimension by the constraint $M_1 \leq M_2$. For the final ages of all the models in the grid, we take the accepted value of the age of the cluster, $t_{\rm H11} = 11.7$ Gyr (Li et al. 2013).

Any stars that evolve off the main sequence before $t_{\rm H11}$ are terminated, and no BSS result is assigned to these initial conditions. This defines a TAMS edge to our parameter space. Although there may be some rejuvenation of the core with hydrogen during a collision, any collisions where one component is beyond the TAMS (Hertzsprung gap or later) will still have a substantial core, and the BSS is therefore expected to remain an evolved star after the collision (Portegies Zwart and Verbunt 1996; Portegies Zwart et al. 1997b). The lack of a need to explore evolution at, or beyond, the Hertzsprung gap has an advantageous side-effect of reducing the computational time, as stars start to undergo rapid structure changes at this point in their evolution and the calculations of their evolution in MESA slows down considerably.

After removing samples that produce no BSS model (for example, where the BSS leaves the main sequence before $t_{\rm H11}$, or initial conditions where $M_2 > M_1$) the number of unique initial conditions that produce a BSS is 1490. Finally, to use the grid for comparison with the observed data, we convert the properties of the simulated model to V and $V-I$ magnitudes using the method in Section 5.2.1. We will describe the results of applying our grid to the observed BSS in Section 5.3.

#	F555W	σ_{F555W}	F814W	σ_{F814W}	V−I	$\sigma_{\mathrm{V-I}}$
1	**20.58**	**0.019**	**20.45**	**0.022**	**0.125**	**0.029**
2	21.17	0.014	20.87	0.013	0.300	0.019
3	21.14	0.014	20.51	0.011	0.633	0.018
4	21.22	0.017	20.63	0.012	0.587	0.021
5	21.03	0.044	20.43	0.038	0.605	0.058
6	21.49	0.020	21.24	0.016	0.241	0.026
7	**21.26**	**0.015**	**20.95**	**0.015**	**0.303**	**0.021**
8	21.97	0.026	21.66	0.022	0.312	0.034
9	22.02	0.063	21.60	0.066	0.415	0.091
10	22.32	0.029	21.89	0.028	0.436	0.040
11	22.59	0.031	22.21	0.038	0.378	0.049
12	**21.53**	**0.022**	**21.14**	**0.016**	**0.389**	**0.027**
13	22.17	0.024	21.71	0.022	0.457	0.033
14	22.32	0.030	21.90	0.025	0.416	0.039
15	21.99	0.022	21.62	0.021	0.366	0.030
16	21.51	0.016	21.09	0.015	0.416	0.022
17	21.69	0.019	21.16	0.016	0.530	0.025
18	22.15	0.029	21.74	0.024	0.409	0.038
19	22.11	0.026	21.69	0.024	0.417	0.035
20	22.07	0.025	21.62	0.024	0.447	0.035
21	22.26	0.031	21.81	0.024	0.452	0.039
22	22.02	0.056	21.51	0.055	0.509	0.078
23	**22.57**	**0.031**	**22.23**	**0.031**	**0.336**	**0.044**
24	**21.77**	**0.019**	**21.52**	**0.049**	**0.252**	**0.053**
25	21.63	0.020	21.17	0.017	0.460	0.026
26	**22.23**	**0.027**	**21.78**	**0.030**	**0.445**	**0.040**
27	**21.95**	**0.022**	**21.43**	**0.019**	**0.516**	**0.029**

Table 5.1: Observed magnitudes in *Hubble Space Telescope* WFPC2 bands, and their errors, for the inner blue straggler stars in Hodge 11. Stars that were used in our MCMC runs are shown in bold.

5.2.3 MCMC approach

Our approach here starts by defining the end point in parameter space, which includes the observed V and I magnitudes of the BSS and the current age of the globular cluster, $t_{\rm H11}$, as well as the errors on these values. We then select the masses of the two stars, M_1 and M_2 ($M_2 \leq M_1$) as well as a collision time $t_{\rm col}$ ($t_{\rm col} < t_{\rm H11}$), and create a BSS model from these initial parameters as outlined in Section 5.2.1. A goodness of fit of the final BSS model is then performed by comparing the model V, $V-I$ and age with the observed parameters, weighted by the observational error in each parameter. A Markov Chain is used to iteratively repeat this calculation, in which M_1, M_2 and $t_{\rm col}$ are selected from the allotted parameter space until we have a consistent match with the observed BSS.

The MCMC analysis was performed using the `python` code `emcee` (Foreman-Mackey et al. 2013). Our MCMC code was constructed to also accommodate fast tests (using simple Gaussian functions rather than the full BSS simulations), in order to first confirm that the method is working as expected (that is, it can correctly reconstruct the original parameters used in the Gaussian distributions). The algorithm used in `emcee` employs an ensemble of 'walkers' that concurrently sample the parameter space at each step in the Markov Chain. Foreman-Mackey et al. (2013) recommend that a large number of walkers are used, although the number of walkers running in parallel is limited in practice by available computational resources. For the results presented here, we used 64 walkers, which we found gave convergence in a reasonable number of steps; the burn-in of the chain, after which the statistics should not be affected by the initial positions of the walkers, was typically only ~ 50 steps.

For the MCMC approach, the final age of the star is now taken as a fitted parameter, as in fact the age of the cluster has some error derived from isochrone fitting: $t_{\rm H11} = 11.7^{+0.2}_{-0.1}$ Gyr. In the MCMC runs, the BSS models are run up to an age of $t_{\rm H11} + 5\sigma^{+}_{t_{\rm H11}} = 12.7$ Gyr (provided that they have not left the main sequence by this time), and the age of the BSS is used in the goodness of fit for a track on the color-magnitude diagram between $t_{\rm H11} \pm 5\sigma_{t_{\rm H11}}$. If the BSS leaves the main sequence after $t_{\rm H11} - 5\sigma^{-}_{t_{\rm H11}}$ but before $t_{\rm H11} + 5\sigma^{+}_{t_{\rm H11}}$, the evolution is stopped at the moment it leaves the main sequence and the goodness of fit is performed on the track between $t_{\rm H11} - 5\sigma^{-}_{t_{\rm H11}}$ and the time it leaves the main sequence.

For the MCMC chains, we constrain the walkers within the parameter space to physically reasonable values of the initial parameters M_1, M_2 and $t_{\rm col}$. For initial conditions where any of these values are less than zero, where $M_1 < M_2$ or where $t_{\rm H11} < t_{\rm col}$, the log prior is set to $-\infty$. Similarly, a very conservative upper bound is placed on the initial masses to prevent walkers performing calculations in an unreasonably high set of initial masses. To obtain a rough estimate of the mass of the BSS, the mass-luminosity relation is used, based on the luminosity of the star (derived from the dereddened V–band magnitude and distance modulus) using $M_{\rm BSS,est} = (L/L_{\odot})^{1/3.88}\ M_{\odot}$. If the sum $M_1 + M_2$ exceeds the conservative limit of $5\ M_{\rm BSS,est}$ in the walker initial conditions, the collision component masses are flagged as being too large, the posterior is

again automatically set to $-\infty$ and the full BSS simulation does not run for this step. For any initial conditions where a star leaves the main sequence, the evolution is also terminated (as per the reasoning in Section 5.2.2) and the log posterior is set to $-\infty$.

Finally, our code catches the rare cases where any of either of the `AMUSE` community codes fails; for example, in the case of not converging on a result in `MMAMS`, or in the case the mass becomes too low for `MESA` to initialise ($\lesssim 0.1\ M_\odot$). To keep the runs fault-tolerant, such exceptions are caught and the code assigns $-\infty$ to the posterior probability, and then the next iteration is initiated.

For successful blue straggler models, the posterior required by `emcee`, in logarithmic form, is the sum of the log of the prior and the log of the likelihood. A naïve prior choice may be the estimated initial mass function of Hodge 11. However, the mass function in the centre of the cluster after core collapse, where it is suggested that collisions are more common, may be of a different form. Therefore, for the current work, the prior on all parameters in `emcee` is taken to be flat, implying a log probability of 0 in all cases.

The log likelihood is calculated from our simulation results and observational data using

$$\frac{1}{2}\sum_i \frac{(X_i - O_i)^2}{\sigma_i^2} - \ln\left(2\pi\sigma^2\right), \tag{5.1}$$

where X is the value of the parameter determined from the simulation, O is the observed value of the parameter, and σ is the error in the observed value.[2] The likelihood is calculated based on three final parameters compared between the simulations and observations (with errors): the V and $V-I$ magnitudes (calculated as outlined in Section 5.2.1) and the age.

We have additionally created a parallelised MCMC code using a distributed version of `AMUSE` (Drost et al. 2012), in order speed up the calculations, where we are able to take advantage of the parallel stretch-move capabilities of the `emcee` package. This enables the walkers to be assigned across not just multiple cores on one machine, or across nodes of a cluster, but on any networked resource that can run the `AMUSE` code.

Table 5.1 shows the inner 27 BSSs in Hodge 11, with the BSSs selected for our MCMC investigations in bold. These stars were chosen in order to test a wide region of the colour-magnitude space of the sample of BSSs. Fig. 5.1 shows the BSSs on the CMD, where the inner and outer blue stragglers are shown as bullets and open circles, respectively.

[2]Note that the maximisation of likelihood is found by the relative differences in the value from equation (5.1). Therefore, when comparing likelihoods, the factor of 1/2 and the second term containing only σ will cancel across trials, and so in practice this is equivalent to simply comparing $\sum_i (X_i - O_i)^2/\sigma_i^2$.

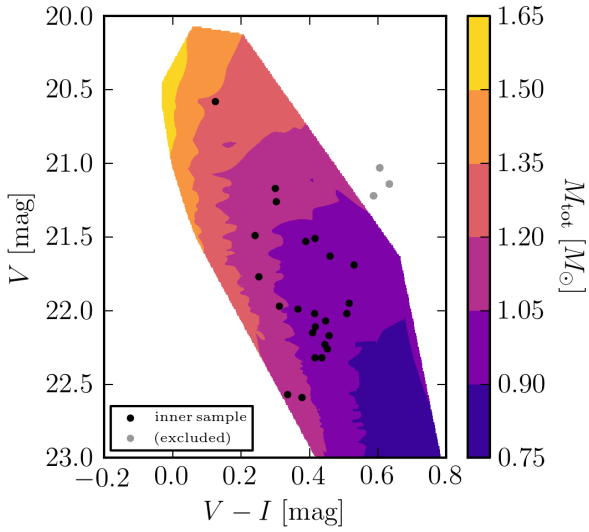

Figure 5.2: Contours of total mass $M_{\rm tot} = M_1 + M_2$ of the two merging component stars located in the observational colour-magnitude space. The points represent the innermost 27 BSSs, where the three grey points are the stars excluded from our analysis as they sit beyond the TAMS.

5.3 Results

We begin this section by considering the results from fitting the grid of simulated BSSs to the observed BSS populations. We then consider the results from the approach of using MCMC searches for the most likely collision components of individual BSSs.

5.3.1 Grid results

Once the grid was generated and converted to observational values (using the method in 5.2.2), we performed a best-fit of the observational data to the grid results. The results from the grid were interpolated, and the best-fit was then carried out by minimising equation (5.1) using the observed and simulated values of the two parameters V and $V - I$.

Our grid results showed that the V and $V - I$ values are generally degenerate in M_1 and M_2, implying that the division of total mass between the two colliding stars does not strongly influence the final position of the BSS on the CMD. Despite this degeneracy, we did still find a rough trend from low to high mass for each of M_1 and M_2, from the lower right to upper left of the CMD. Reflecting the trends seen in the individual masses, the *total* mass $M_{\rm tot}$ has a more clearly defined result in V and $V - I$, and this is shown in Fig. 5.2.

The value of $t_{\rm col}$ is also well defined in V and $V - I$, and we show contours of the grid results in Fig. 5.3. Fitting the inner 24 BSSs that sit within the grid results for $t_{\rm col}$ (black points in Fig. 5.3) allows us to generate a cumulative distribution function (CDF) of collision times found from this method, and this is shown in Fig. 5.4. To compare with the CDFs of collision times from the grid data, we investigate two pos-

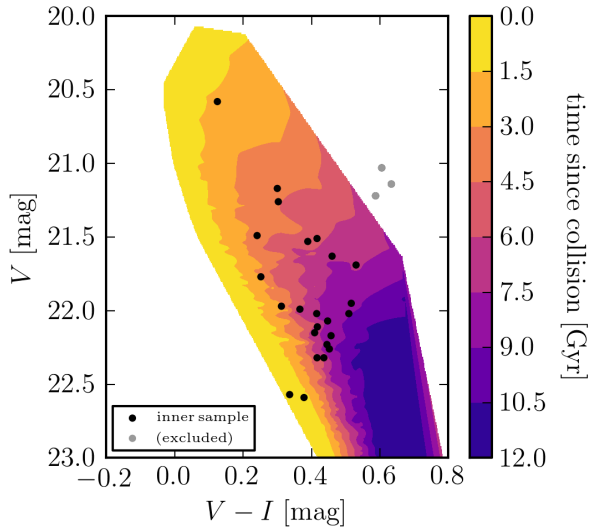

Figure 5.3: Contours of collision time $t_{\rm col}$ located in the observational colour-magnitude space. The points represent the innermost 27 BSSs, where the three grey points are the stars excluded from our analysis as they sit beyond the TAMS.

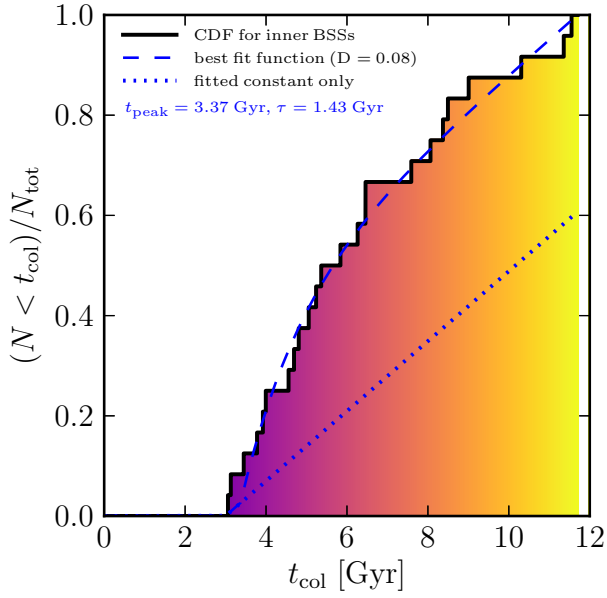

Figure 5.4: Cumulative distribution function (CDF) of $t_{\rm col}$ for the inner BSSs fitted from the grid data (as shown in the contours of Fig. 5.3). The colour under the CDF corresponds to the same colouring in the contours of Fig. 5.3. The solid blue line shows the best-fit exponential function (on top of a constant background) for collision probability. The dotted blue line shows the constant background to this fit alone.

sible fitting functions. In each case, we assume that BSSs formed from other channels (such as binary mass transfer) produce a signal in these results equivalent to a constant background rate for formation. Therefore, we try fitting the CDF with two components: a function representing the time-dependent formation probability via collisions, and a time-independent background probability.

For our fit, we used an exponentially decaying probability of collision, decaying from a time $t_{\rm peak}$, with a decay time constant (e-folding time) τ, on top of a time-independent background probability, c. Due to the cut-off in observed BSS in our sample at ~ 3 Gyr, an additional filter is applied to the fitting functions where any BSS formation rate below this observational cut-off, $t_{\rm min}$, is set to 0. The fitting function is, therefore,

$$p_{\rm col}(t) \equiv \begin{cases} 0 & t < t_{\rm min} \\ c & t_{\rm min} \leq t < t_{\rm col} \\ b \exp\left(\left(t_{\rm peak} - t\right)/\tau\right) + c & \text{otherwise .} \end{cases} \tag{5.2}$$

Note that we do not impose any constraint in any of the fitting that requires $t_{\rm col} > t_{\rm min}$, only that all parameters must be positive. To find the best fit to the CDFs for these functions, we use a Nelder-Mead simplex optimisation to find the minimum Kolmogorov–Smirnov (KS) statistic over the free parameters $t_{\rm peak}$, τ, b and c.[3]

The best-fit exponential function is overlaid on the data in Fig. 5.4, as well as the constant background from this fit as a dotted line. The parameters of the best-fit exponential component are shown in the figure; the constant background corresponds to a formation rate of 1.7 Gyr^{-1}. If we can attribute the constant background to a signal from mass-transfer origins, this suggests that the majority of collisional BSSs formed between 3 and 6 Gyr, where we attribute the peak of exponential component with the core-collapse time of the cluster, $t_{\rm cc} \approx 3.4$ Gyr. By 6 Gyr, the exponential component has contributed two-thirds of the total BSS formation. By the age of the cluster, the formation of BSSs from the constant background becomes the dominant contribution (~ 60 per cent of the total).

5.3.2 MCMC results

An example of MCMC walker positions for a specific inner BSS, number 1 in Table 5.1, is shown in Fig. 5.5. It is evident from Fig. 5.5 that the positions of the walkers (and therefore the statistics derived from them) after step ~ 70 are not affected by the

[3]We also considered an alternative fitting function to model a burst of BSS formation modelled by a Gaussian, centred on $t_{\rm col}$ with a width of σ, on top of a constant background probability, c. We found that, after optimisation, both functions can fit the data equally well; however, the best-fit Gaussian requires a large dispersion ($t_{\rm peak} = 3.4$ Gyr, $\sigma = 1.8$ Gyr). This, therefore, implies that a narrow burst of formation does not describe these results—and, in agreement with the exponential distribution, a gradually decaying formation probability provides a better model.

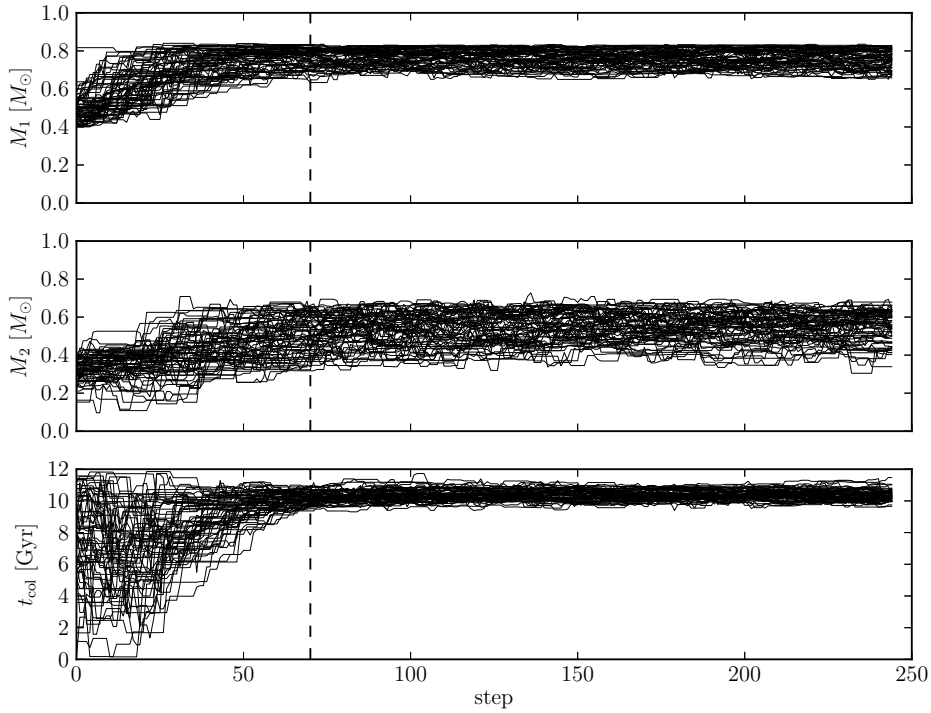

Figure 5.5: Positions of walkers used for the MCMC run for inner BSS 1. The parameters from top to bottom are: the mass of the more massive star, the mass of the less massive star, and the collision time. The black dashed line shows the cut for the chain burn-in; positions prior to this are not used for the final statistics.

initial positions of assigned to the chain. We therefore discard the first 70 steps as burn-in values for the chain, and produce results from the remaining steps. For the other MCMC runs, we use the same approach for finding a burn-in position.

A triangle plot, showing the samples for the MCMC run of the same example BSS (number 1), is presented in Fig. 5.6, to illustrate relationship between the three parameters M_1, M_2 and $t_{\rm col}$. These distributions are based on the positions of all the walkers in parameter space after removing the burn-in of 70 steps. We overlay three dashed lines on the distributions corresponding to the $16^{\rm th}$ percentile, the median and the $84^{\rm th}$ percentile of the distributions (to be compared with the parameter and σ estimates in Table 5.2).

Table 5.2 shows the results from all our MCMC runs. In general (as shown for the specific example of BSS 1), we find that the value of $t_{\rm col}$ is better defined than M_1 and M_2. This is in agreement with the results from the grid, which showed that although the total mass of the merging stars was better defined, there was degeneracy in the distribution of that mass between M_1 and M_2.

BSS #	steps	M_1	$\sigma^-_{M_1}$	$\sigma^+_{M_1}$	M_2	$\sigma^-_{M_2}$	$\sigma^+_{M_2}$	$t_{\rm col}$	$\sigma^-_{t_{\rm col}}$	$\sigma^+_{t_{\rm col}}$	grid $t_{\rm col}$
1	245	0.77	0.04	0.06	0.55	0.08	0.10	10.34	0.38	0.33	10.31
7	136	0.68	0.09	0.09	0.43	0.10	0.13	7.59	0.59	0.48	7.59
12	146	0.66	0.09	0.08	0.38	0.10	0.13	6.22	0.71	0.67	6.46
23	139	0.66	0.08	0.08	0.40	0.10	0.12	9.04†	2.49	1.65	11.55
24	168	0.68	0.08	0.08	0.44	0.08	0.11	8.63	1.50	1.68	9.01
26	201	0.63	0.09	0.09	0.35	0.10	0.11	4.63‡	1.99	1.46	3.99
27	155	0.59	0.10	0.08	0.36	0.09	0.13	3.25	0.79	0.73	3.13

Table 5.2: Results of MCMC search for the collision components of selected innermost BSSs. All MCMC chains used 64 walkers per step. The first column gives the BSS number corresponding to the first column of Table 5.1. Masses are in units of $M_\odot$ and collision times are given in units of Gyr. The 'steps' column corresponds to the number of MCMC steps in the chain used in determining these results, including the burn-in values (which ranged from $40 \sim 70$ steps). The final column shows the best-fit value of $t_{\rm col}$ from the grid results for comparison. †: shows strong bimodality in the result for $t_{\rm col}$ (therefore the median value should be taken with caution); ‡: shows mild bimodality in $t_{\rm col}$

In Table 5.2 we also list the best-fit value of $t_{\rm col}$ obtained from the grid results. Comparing the results for $t_{\rm col}$ determined from the grid interpolation with those found in the MCMC runs shows good agreement between the two techniques (except for multi-modal solutions affecting the median value). The general agreement of the MCMC results with the grid interpolation provides confirmation of the effectiveness of our MCMC approach in finding solutions for this problem.

5.3.3 An independent estimate of the core-collapse time

For comparison with our estimate of the core-collapse time ($t_{\rm cc} \approx 3.4$ Gyr), we consider an independent means of estimating $t_{\rm cc}$ described in Pijloo et al. (2015). This technique uses the observed conditions of clusters as fitting parameters for another MCMC method, which is based on a parametrised cluster evolution code (`EMACSS`; Alexander and Gieles 2012).

The cluster mass, galactocentric radius, velocity at this radius, and half-light radii are all used as fitting parameters for this approach. For Hodge 11, the first three of these parameters were respectively taken from Suntzeff et al. (1992), Freeman and Gascoigne (1977) and Alves and Nelson (2000). A range of possible (projected) half-light radii were considered, $2 \text{ pc} \leq r_{\rm phl} \leq 4$ pc, as this value is somewhat uncertain in the literature for Hodge 11.

Core-collapse was found to be around, or before, ~ 3 Gyr for simulations with $r_{\rm phl} \lesssim 3.7$ pc (T. Pijloo, personal communication, 2015). There is then a large jump to $t_{\rm cc} \sim 8$ Gyr found for half-mass radii only 10 per cent larger. Although there is no clear trend in $t_{\rm cc}$ with the (uncertain) half-light radius, the early core-collapse times that are found at small half-light radii are broadly consistent with our previous estimate. Inverting the problem, if we take our predicted core-collapse time to be true, the core-collapse times found using this independent method suggest that the half-light radius

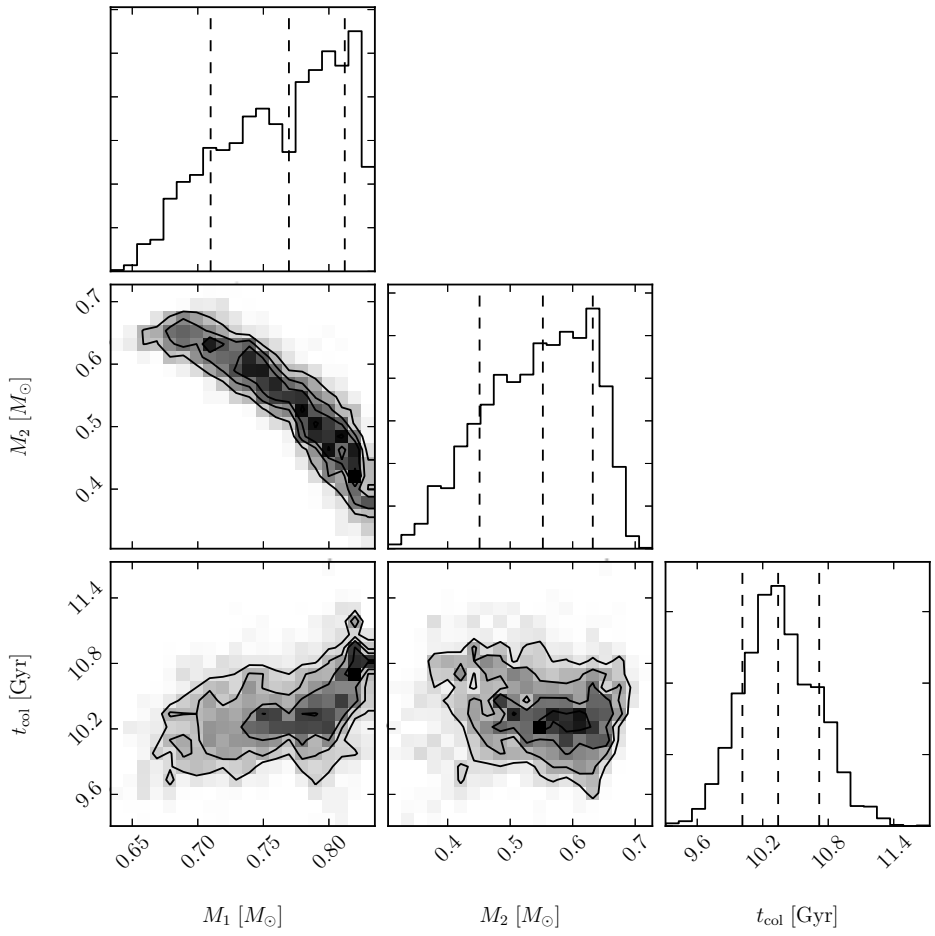

Figure 5.6: Triangle plot showing the outcome of MCMC sampling for inner BSS 1. M_1 and M_2 are the collision component masses, and $t_{\rm col}$ is the collision time. The vertical dashed lines show the median value, with the $16^{\rm th}$ and $84^{\rm th}$ percentiles on either side. These results were produced with 64 walkers, after removing 70 burn-in steps.

of Hodge 11 must be $r_{\rm phl} \lesssim 3.7$ pc in order to agree with this value.

5.4 Discussion and conclusions

The 11.7 Gyr–old globular cluster Hodge 11 in the Large Magellanic Cloud has a rich population of blue stragglers. A total of 54 of these have been studied by Li et al. (2013), who separated them in equal portions of a more centrally concentrated population and a more extended population. They suggest that the inner population resulted from dynamical collisions between stars, whereas the homogeneous population could be the result of mass transfer in binary systems. Here, we examined the same BSSs in order to predict the properties of the collision that would be required to form them, as well as what this can tell us about the dynamical history of the cluster.

Beginning with the innermost BSSs, we adopt the assumption that all blue stragglers are the result of a collision between two stars which, at some moment $t_{\rm col}$, merge to a single star, after which it continues to evolve to the age of the cluster. In attempting to reproduce the observed blue straggler population, we determine the best combination of primary mass, secondary mass and the moment of the collision. Following our conversion of the observed luminosity and colours, several blue stragglers turn out to have already left the main sequence. We excluded those from our analysis, leaving our fitting procedure with 24 of the innermost BSSs, which reside in a region where collisions have been argued to be more likely.

The procedure was carried out with the stellar evolution code `MESA` (Paxton et al. 2011) to evolve the two stars to the collision time, and we adopt the Make-Me-A-Massive-Star entropy-sorting algorithm (Gaburov et al. 2008) to carry out the stellar collisions. After the collision calculation is completed, we continue the evolution of the resulting single star using `MESA`. The code coupling was realised with the Astronomical Multipurpose Software Environment (Portegies Zwart et al. 2013a). A critical step of comparing our simulation results with observations is the conversion of the parameters from the stellar evolution calculations to the HST magnitudes, which is achieved by convolutions of the HST response functions with the best-fit synthetic spectra.

We have carried out the analysis in two different ways: by calculating a grid of primary masses, secondary masses and collision times, and by a Markov Chain Monte Carlo method. In the former analysis, we notice that the individual stellar masses tend to be rather unconstrained. The Markov Chain calculations indicate that this is caused by the degeneracy in the masses of the primary and secondary stars. The total stellar mass provides a better defined parameter, whereas the mass ratio can vary over a much wider range. The collision time can also be determined quite distinctly for each blue straggler, and it is in particular this quantity that we interpret.

By fitting the CDF of the collision times, we recognise two contributions to BSS formation: a constant BSS formation rate of ~ 1.7 Gyr^{-1}, which we tentatively attribute to the effect of binary mass transfer and coalescence, and an exponential decay peaking at 3.4 Gyr and with an e-folding time of 1.4 Gyr, which we attribute to col-

lisions originating from the core collapse of the cluster. The decay time scale in the exponential may then be attributed to the multiple collapses in the period following the main core collapse. These gravothermal oscillations (or core oscillations, depending on the details of the gravothermodynamics) can last for time scales of $\sim$ Gyr, which is consistent with our derived decay time scale (see, for example, Breen and Heggie 2012, and references therein).

We also performed a two-sample KS test between the CDFs obtained by fitting the individual innermost and outermost BSS subsamples to the grid independently. The KS statistic for these two distributions is $D = 0.32$; with the given sample sizes, this corresponds to a p-value of 0.16, which does not support rejecting the null hypothesis that the two samples are drawn from the same population. Alternatively, under the assumption that our best-fit distribution for the innermost BSSs represents the true formation probability, we also performed a one-sample KS test for the CDF of the outermost BSSs against this distribution.[4] As expected, this gives a similar statistic of $D = 0.29$. With the sample size of 21 inner BSS that lie on the grid, the p-value is 0.051; this is a stronger result, though not quite significant at the 5 per cent level. Therefore, in the framework of the current analysis—that is, based on fitting to $t_{\rm col}$ from collisional models alone—our results cannot rule out the hypothesis that the same mechanisms (and therefore $t_{\rm col}$ distributions) govern the origin of the innermost and outermost BSSs.

A caveat to this approach is the cut-off used to determine the BSS star population used in Li et al. (2013). In order to be considered a BSS, a star had to be more than 3σ away from the (isochrone-fitted) ridge-line of the cluster. This likely omits some BSSs created by collisions that are within 3σ of the ridge-line, and therefore some stars that correspond to the earliest collision times (see Fig. 5.4) will be missed in the sample.

Inverting the cluster evolution, using the observed parameters, an MCMC search with a parametrised cluster evolution code can be used to provide an alternative estimation of the core-collapse time (Pijloo et al. 2015). The moment of core collapse in this reconstruction is uncertain, and is quite sensitive to the cluster half-light radius; the prediction that the cluster has indeed undergone core-collapse within its lifetime, however, is more robust. Within the limitations of this analysis, the results suggest Hodge 11 experienced core collapse $\lesssim 3$ Gyr after birth if the half-light radius is sufficiently low ($3 \sim 4$ pc).

Both of our approaches to estimating collision components of BSSs have some uncertainty due to degeneracy. In the case of the grid, although a much clearer trend was evident in $t_{\rm col}$ and $M_{\rm tot}$ than (separately) M_1 and M_2, there was still some overlap on colour-magnitude space in some of these results, which results in some uncertainty in the interpolation. In the case of the MCMC chains, degeneracy is not only seen in M_1 and M_2 especially, but there is also evidence for bimodality in some solutions for $t_{\rm col}$ as shown in Fig. 5.7 (and therefore averaging should be treated with caution).

[4] That is, the parameters of the tested distribution are *not* derived from the sample data, as we are now comparing a different subsample of the BSS population.

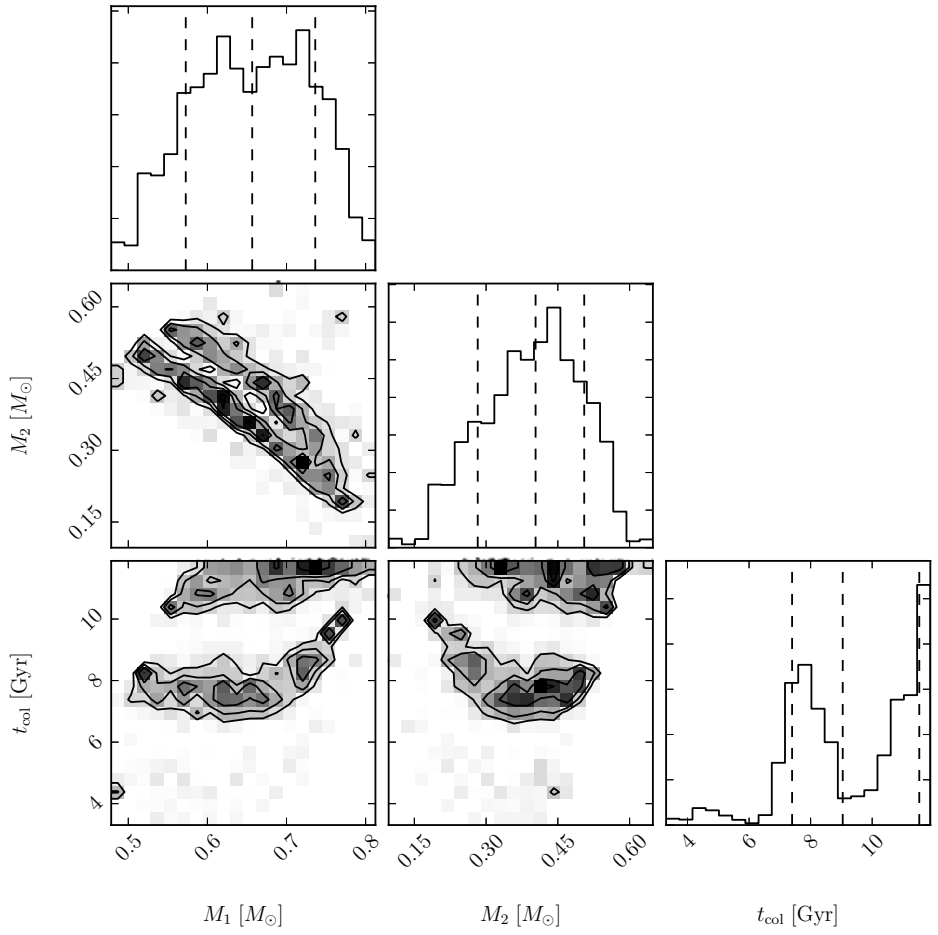

Figure 5.7: Triangle plot showing the outcome of MCMC sampling for inner BSS 23. This example has been included to show the clear bimodality in $t_{\rm col}$ for this result (the strongest case of bimodality out of all BSSs considered). Parameters and markers are the same as for Fig. 5.6. These results were produced with 64 walkers, after removing 50 burn-in steps.

Some multi-modality seen in the results is due to the inherent gridding in producing V and $V - I$ from the stellar models (even in the MCMC solutions) due to the finite library of stellar spectra used in the conversions from the stellar models.

A final caveat in this analysis is that the binary mass-transfer population is probably better modelled by adding mass to the stellar surface of the emerging blue straggler, rather than by applying the adopted entropy sorting algorithm, and the details of our conclusions may be affected by this. However, we do not know beforehand which blue stragglers are formed via one channel or the other, and therefore it would be somewhat complicated to invoke two formation scenarios. It would, nevertheless, in principle, be possible to conduct a primary component and optimization algorithm to the two distinct populations, taking into account the inner and the outer binary conditions. This would be a computationally intensive and rather uncertain undertaking without a guarantee that it provides a unique answer to the question of how the two populations are (or should) be divided among the individual blue stragglers. We therefore currently limit our analysis to the method described.

Our work shows that this method applied to BSS samples in other environments can be used to infer cluster dynamical evolution. This method is complementary to other techniques that use BSSs as a 'dynamical clock', such as inferring the current dynamical state of a cluster from the radial distribution of BSSs (Ferraro et al. 2012). As we could not rule out the hypothesis that the outermost BSSs in Hodge 11 come from the distribution that describes the innermost BSSs, a possible explanation is that collisional BSSs formed from an early core collapse may percolate to larger radii. Therefore, caution should be exercised when making a distinction of formation channels using radial positions of BSSs alone.

Acknowledgements

This work was supported by the Netherlands Research Council (NWO grant numbers 612.071.305 [LGM] and 639.073.803 [VICI]) and by the Netherlands Research School for Astronomy (NOVA). We are grateful to Carmen Martínez-Barbosa for providing us with her code for generating magnitudes from from BaSeL spectra and for instructing us on its use. We also thank Tjibaria Pijloo for supplying core-collapse estimates for Hodge 11, as well as Chengyuan Li and Richard de Grijs for supplying data on the BSSs in Hodge 11.